Chapter 3: Result and discussion- Photocatalytic and photo-electrochemical study

3.1 Photocatalysis Study

3.1.3 Results and Discussion

The size and structure of synthesized $BiVO_4$, ZnO and ZnO-$BiVO_4$ nanocomposite powder were investigated by transmission electron microscope. Fig 3(a) shows the clear formation of $BiVO_4$ nanoparticles with average size of 40-100 nm. It was observed that particles were aggregated which may be due to their self-assembly during TEM grid drying process. TEM image illustrates the overlapping ZnO nanosheets with size considerably varying from few hundred to several hundred nanometres as shown in Fig 3(b). Nanocomposite TEM micrograph in Fig 3(c) & (d) shows two distinct morphologies of ZnO nanosheets and $BiVO_4$ nanoparticles, also showing the incorporation of latter into former which confirms the successful formation of ZnO-$BiVO_4$ (1:1) nanocomposite. Fig 3(e) shows the EDS of the ZnO-$BiVO_4$ nanocomposite and confirms the presence of Zinc, Bismuth, Vanadate and Oxygen. Copper peak is due to the copper grid used in TEM sample preparation.

More TEM images showing complete attachment of $BiVO_4$ nanoparticles to ZnO nanosheets at lower magnification scale is shown in Fig 3.2.

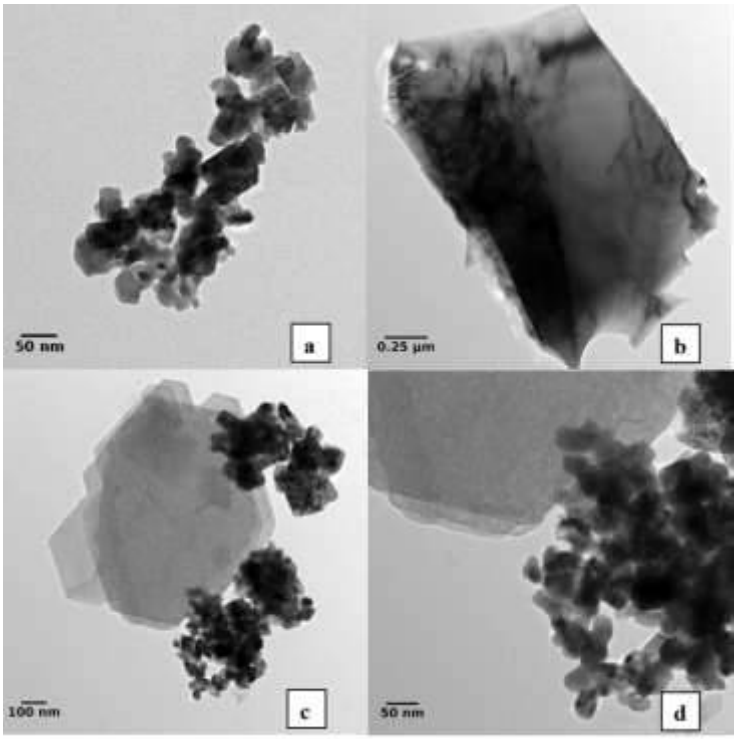

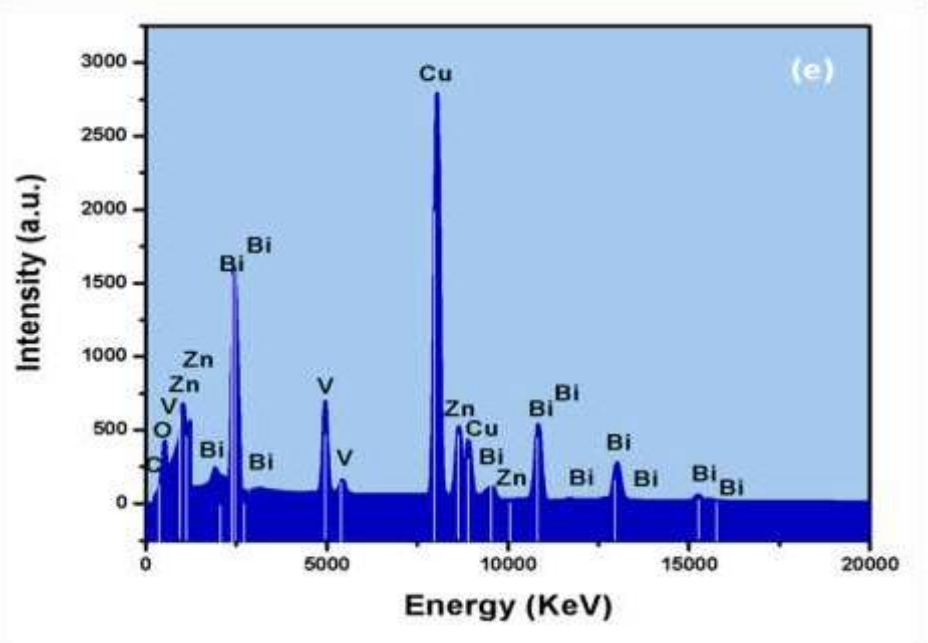

Fig 3.1 TEM micrograph of (a) $BiVO_4$ nanoparticles, (b) ZnO nanosheets (c) & (d) $ZnO/BiVO_4$(1:1) nanocomposite (e) EDS for ZnO-$BiVO_4$(1:1) nanocomposite

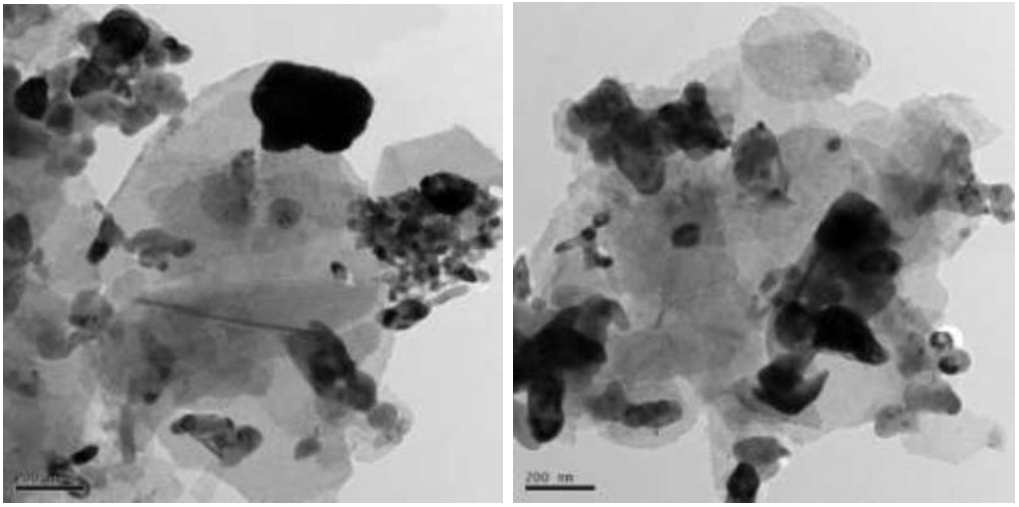

Figure 3.2. TEM images of composite samples revealing complete attachment of $BiVO_4$ nanoparticles to ZnO nanosheets at lower magnification scale

Fig 3.3 shows the XRD patterns of $BiVO_4$, ZnO, ZnO-$BiVO_4$ (1:1) nanocomposite. All the peaks of ZnO and $BiVO_4$ in Fig 3.3 (a) and (b) are in good match with JCPDS card No.36-1451 and 83-1699 respectively. The calculated values of lattice parameters of ZnO (a=3.25 Å, c=5.2 Å) and $BiVO_4$ (a=5.189 Å, b=5.080 Å, c=11.73 Å, γ= 90.41^{O}) were found to be consistent with the standard values confirming the wurtzite hexagonal and monoclinic crystal structure respectively. XRD diffractogram for ZnO-$BiVO_4$ nanocomposite, Fig 3.3(c), exhibited characteristic peaks of both ZnO and $BiVO_4$. There was no change in phase of both the materials in nanocomposite rather a change in crystallinity was observed as evidenced from the change in FWHM values. In case of ZnO nanosheets, values of FWHM for the planes (100), (002), (101) changes from 0.56, 0.46, 0.62 to 0.45, 0.34, 0.6 radian, respectively, which shows an increase in crystallite size whereas in $BiVO_4$ FWHM values corresponding to the plane (121), (114) changes from 0.38, 0.58 to 0.64, 0.82 radian respectively which indicates the decrease in crystallite size.

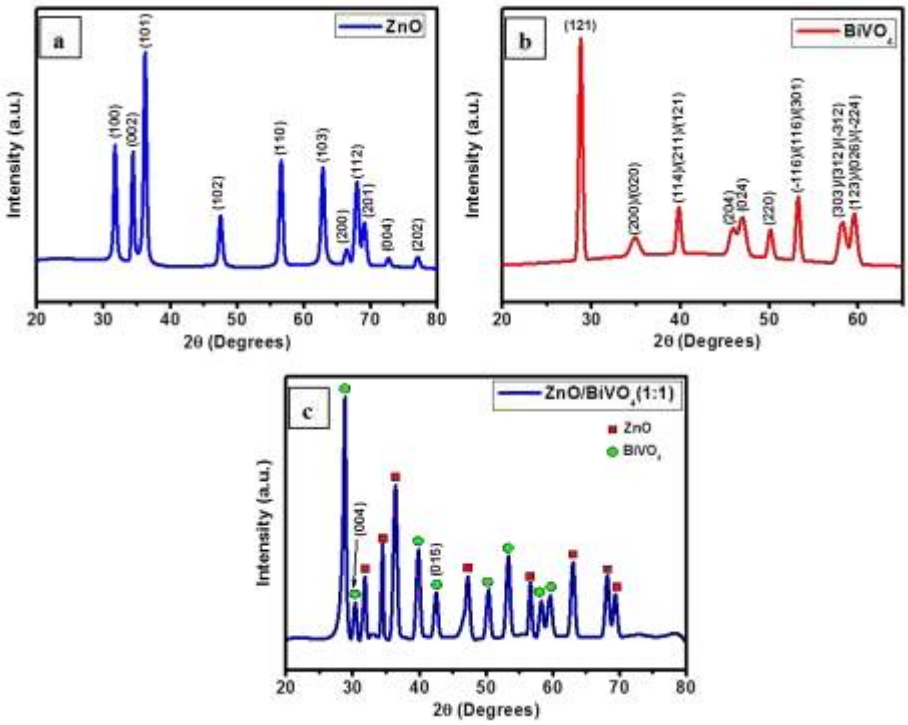

Fig 3.3. XRD spectras of ZnO nanosheets (a), $BiVO_4$ nanoparticles (b) and ZnO/$BiVO_4$ nanocomposite (c).

Further, no distortion in crystal lattice of ZnO and $BiVO_4$ in composite was observed as the calculated values for a_{ZnO}, b_{ZnO} and a_{BiVO4}, b_{BiVO4}, c_{BiVO4}, γ_{BiVO4}, were in good agreement with the corresponding values of the pristine samples, thus indicating no phase change in the composite (Table 3.1). XRD pattern of composite also reveals the formation of two new planes of $BiVO_4$ at (004) and (015), respectively, which were originally not present in pristine sample.

Table 3.1 Crystal Lattice data of ZnO, $BiVO_4$ and ZnO-$BiVO_4$ (1:1)

Sample	**a (Å)**	**b(Å)**	**c(Å)**	**γ (Degree)**
ZnO	3.25	N.A.	5.2	N.A.
$BiVO_4$	5.189	5.080	11.73	90.41
ZnO-$BiVO_4$ (1:1) composite	a_{ZnO}= 3.23 a_{BiVO4} = 5.19	b_{BiVO4}= 4.94	c_{ZnO}= 5.194 c_{BiVO4}= 11.766	γ_{BiVO4}= 90.86

Fig 3.4(a), (b), (c) shows the room temperature PL emission spectra of pure ZnO, pure $BiVO_4$ and ZnO-$BiVO_4$ (1:1) nanocomposite. Near band edge UV emission peak for ZnO was recorded at 383 nm (3.23 eV) and broad green emission peak at 532 nm was observed owing to various oxygen vacancies [194] on sample surface. $BiVO_4$ PL peak at 514 nm (2.4 eV) corresponds to near band edge emission. A shift in PL emission peak was observed in nanocomposite in comparison to pure ZnO sample which is due to the presence of $BiVO_4$ in the sample. A strong PL emission peak was observed at 421 nm (2.94 eV) for nanocomposite which is approximately equal to the energy difference between the valence band (VB) of $BiVO_4$ and conduction band (CB) of ZnO which clearly indicates that maximum electron transition is taking place between these two energy bands. Thus in nanocomposite VB of $BiVO_4$ acts as an intermediate band between VB and CB of ZnO at interface. Due to this intermediate band, the amount of energy required for electrons to jump from VB to CB of ZnO is reduced (2.94 eV) which makes nanocomposite photoactive in visible region.

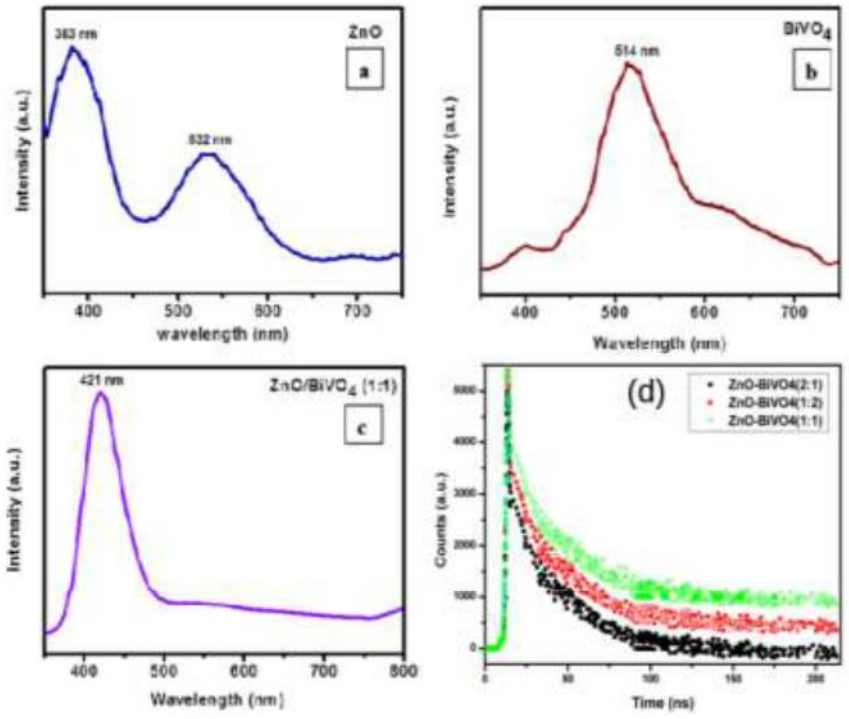

Fig 3.4: Photoluminescence for ZnO nanosheets (a), $BiVO_4$ nanoparticles (b), ZnO-$BiVO_4$ nano-composite (c) and Luminescence decay study (d)

PL decay curves were studied to better understand the recombination process, Fig. 3.4(d). Following equation was used to define the curves fitted with bi-exponential decay response:

where y_o is the baseline correction, t_1 ,t_2 are the decay constants and A_1, A_2 are the pre-exponential factors.

Following formula [195,196] was used to calculate the average decay time, τ_{avg}:

The average lifetime, using above equation, for ZnO-$BiVO_4$ (1:1), ZnO-$BiVO_4$ (1:2), ZnO-$BiVO_4$ (2:1) were calculated to be 37, 27 and 25ns, respectively. ZnO-$BiVO_4$ (1:1) has a increased lifetime compared to ZnO-$BiVO_4$ (1:2), ZnO-$BiVO_4$ (2:1). Several factors affect the lifetime of charge carriers such as carrier trapping, band structure, mobility of charge carriers etc. It was stated by Baiju et al. that the longer lifetime is also the result of interface formation between different materials in interface [40]. So above data clearly indicates the best interface formation in ZnO-$BiVO_4$ (1:1) in comparison to ZnO-$BiVO_4$ (1:2), ZnO-$BiVO_4$ (2:1).

The XPS was obtained to analyze the surface chemical composition and oxidation state of ZnO-$BiVO_4$ nanocomposite and to further study the interaction of ZnO with the $BiVO_4$ support. XPS spectra of O 1s and Zn 2p for pure ZnO and ZnO-$BiVO_4$ heterojunction, as well as the V 2p and Bi 4f spectra for the pure $BiVO_4$ and heterojunction are shown in Fig 3.5. The binding energy values of Zn 2p1/2 and Zn 2p3/2 were observed at 1044.49 and 1021.09 eV (Fig. 3.5a), respectively, which can be accredited to the Zn^{2+} ions of the ZnO after comparing peak positions with Handbook of X-ray Photoelectron Spectroscopy. However, the binding energies of Zn 2p1/2 and Zn 2p3/2 for ZnO-$BiVO_4$ heterojunction were 1044.8 and 1021.6 eV, respectively, which are

higher than those for pure ZnO. The XPS peaks for O 1s (530.19 and 529.79 eV) endured the same binding energies, as shown in Fig. 3.5b. Such chemically shifted peaks of Zn 2p in the heterojunction can be ascribed to the Zn interaction with Bi and V. Furthermore, the emergence of new Bi 4f peak at 157.63 eV (Fig. 3.5d) and the red shift of V2p peak from 519.59 to 516.27 eV (Fig. 3.5c) in composite indeed reveals that the $BiVO_4$ structure has undergone changes after interaction with ZnO to construct a heterojunction, which confirms the presence of interface between ZnO and $BiVO_4$.

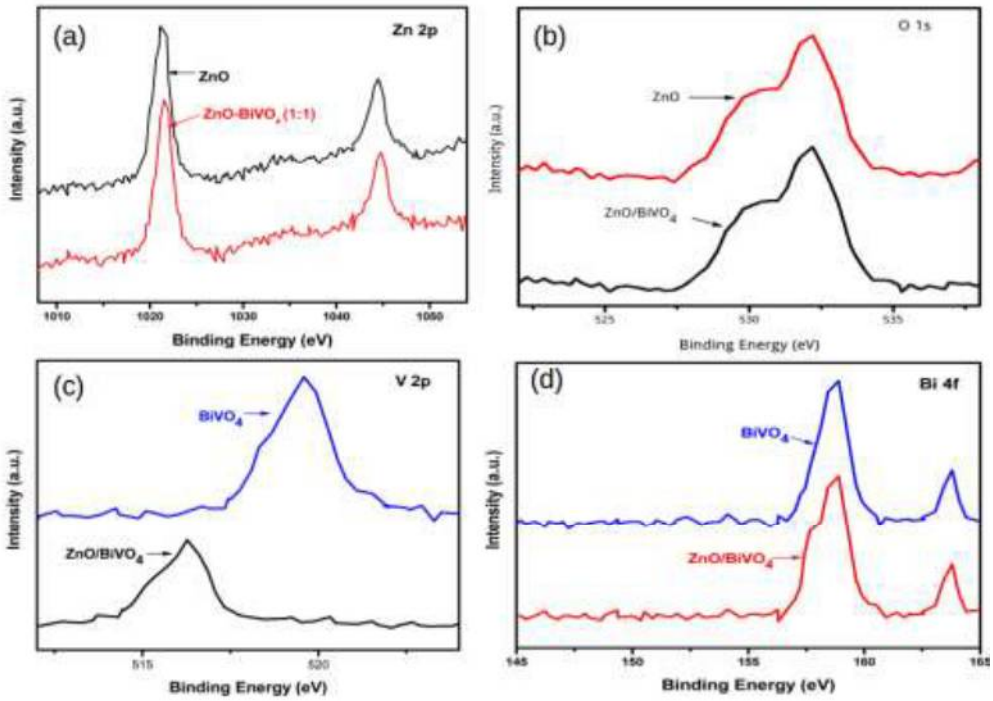

Fig 3.5: XPS spectra for: (a) Zn 2p peak of pure ZnO and ZnO-$BiVO_4$ heterojunction; (b) O1s peak of pure ZnO and ZnO-$BiVO_4$ heterojunction; (c) V 2p peak of pure $BiVO_4$ and ZnO-$BiVO_4$ heterojunction (d) Bi 4fpeak of pure $BiVO_4$ and ZnO-$BiVO_4$ heterojunction

3.1.4 Calculations

3.1.4.1 Estimation of Energy Band Gaps

3.6(a), (b), (c) shows the Tauc's plot for ZnO, $BiVO_4$ and ZnO-$BiVO_4$ (1:1) nanocomposite as calculated from their respective UV emission spectra. Band gap of material was determined using Tauc's plot as obtained by plotting $(\alpha h\upsilon)^{1/n}$ versus $(h\upsilon)$ where α is the absorption coefficient of the

material and n denotes the nature of transition. ZnO and $BiVO_4$ exhibits direct allowed transition for which value of n=1/2 [197,198]. Band gaps were observed to be 3.23 eV, 2.4 eV and 2.94 eV for ZnO, $BiVO_4$ and nanocomposite respectively.

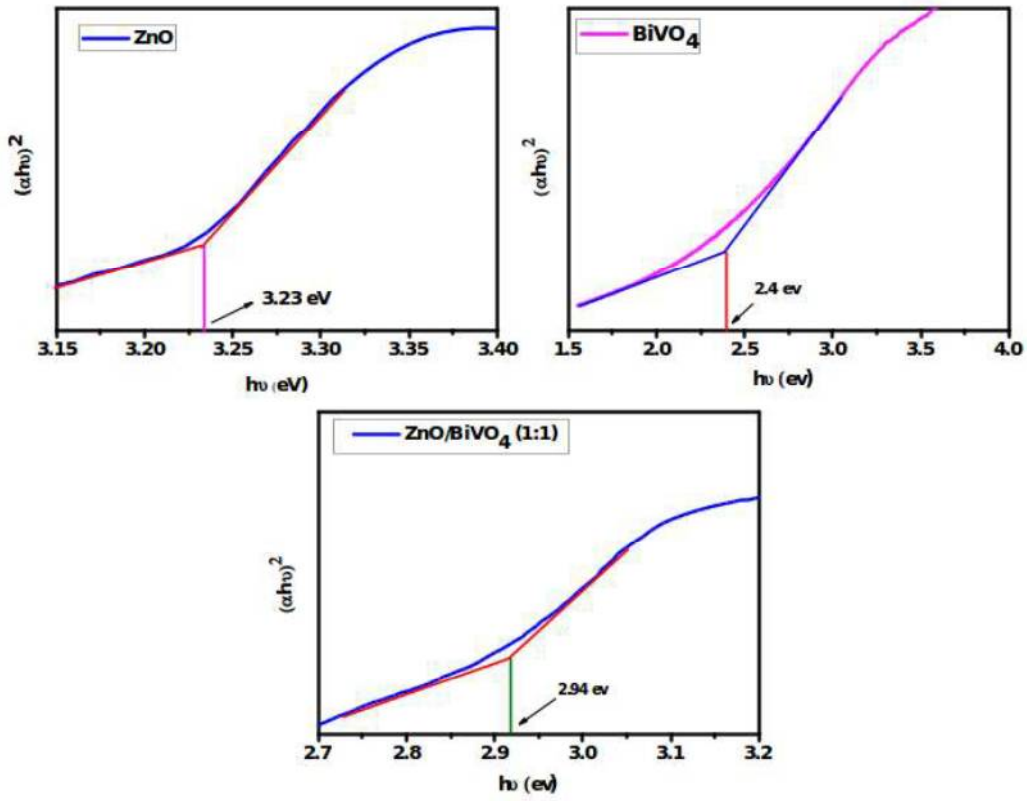

Fig 3.6 Tauc's plot for ZnO nanosheets (a), $BiVO_4$ nanoparticles (b) and ZnO-$BiVO_4$ nano-composite (c)

3.1.4.2 Estimation of Energy Band Edges

The VB and CB band edge positions were calculated using Mulliken Electronegativity theory given by formula:

where E_{VB} is the valence band edge potential, E_{CB} is the conduction band edge potential, X is the absolute electronegativity, E_e is the energy of free electrons which is ~4.5 eV on the hydrogen scale and E_g is the band gap energy of the semiconductor. Value of X for ZnO and $BiVO_4$ is 5.95 and

6.04 eV respectively [199,200]. The E_{CB} of ZnO and $BiVO_4$ are calculated and found to be -0.16 eV and 0.34 eV, respectively. The E_{VB} of ZnO and $BiVO_4$ are estimated to be 3.06 and 2.74eV, respectively. The energy gap between CB of ZnO and VB of $BiVO_4$ almost equals the band gap of the material (~2.9 eV), thus showing that maximum charge transitions are taking place between the two bands as also confirmed from UV and PL studies.

3.1.4.3 DFT computations on the interaction of heterojunction

To investigate the interaction between ZnO and $BiVO_4$ at the heterojunction, DFT calculations were performed on theoretical model of the interface. Based on XRD results, ZnO slab corresponding to (101) plane was considered for calculations. We first investigated the lattice structure of pristine ZnO(101), $BiVO_4$ and ZnO (101)- $BiVO_4$ hetrojunction. Negligible change in atomic coordinates of ZnO(101) and $BiVO_4$ was observed after geometrical optimization. In ZnO(101)-$BiVO_4$ heterojunction, calculated vacuum spacing between ZnO(101) and $BiVO_4$ after geometrical optimization was 2.36 Å (Fig 3.7). It is widely known that close contact between different materials in composite is advantageous for charge transfer and separation

To investigate the enhanced photo-catalytic activity of ZnO(101)-$BiVO_4$ heterojunction we calculated its band structure. Band structures of ZnO(101) and $BiVO_4$ were also calculated for comparison. Band structures are shown in Fig 3.8. ZnO(101) was direct band bap semiconductor with 0.91eV as calculated band gap as shown in Fig 4.8(a) , which is in good agreement with previously calculated results [201,202]. $BiVO_4$ band structure indicated indirect band gap of 2.16 eV with valence band maximum at L-M and conduction band minimum at L as shown in Fig 3.8(b). Calculated band gap of $BiVO_4$ is also in good agreement with previously calculated results [203]. ZnO(101)-$BiVO_4$ hetrojunction had indirect band gap of 1.8eV with valence band maximum at Z and conduction band minimum at G in Fig 3.8(c). The calculated values of band gaps are not reliable [204] due to commonly known shortcoming of DFT.

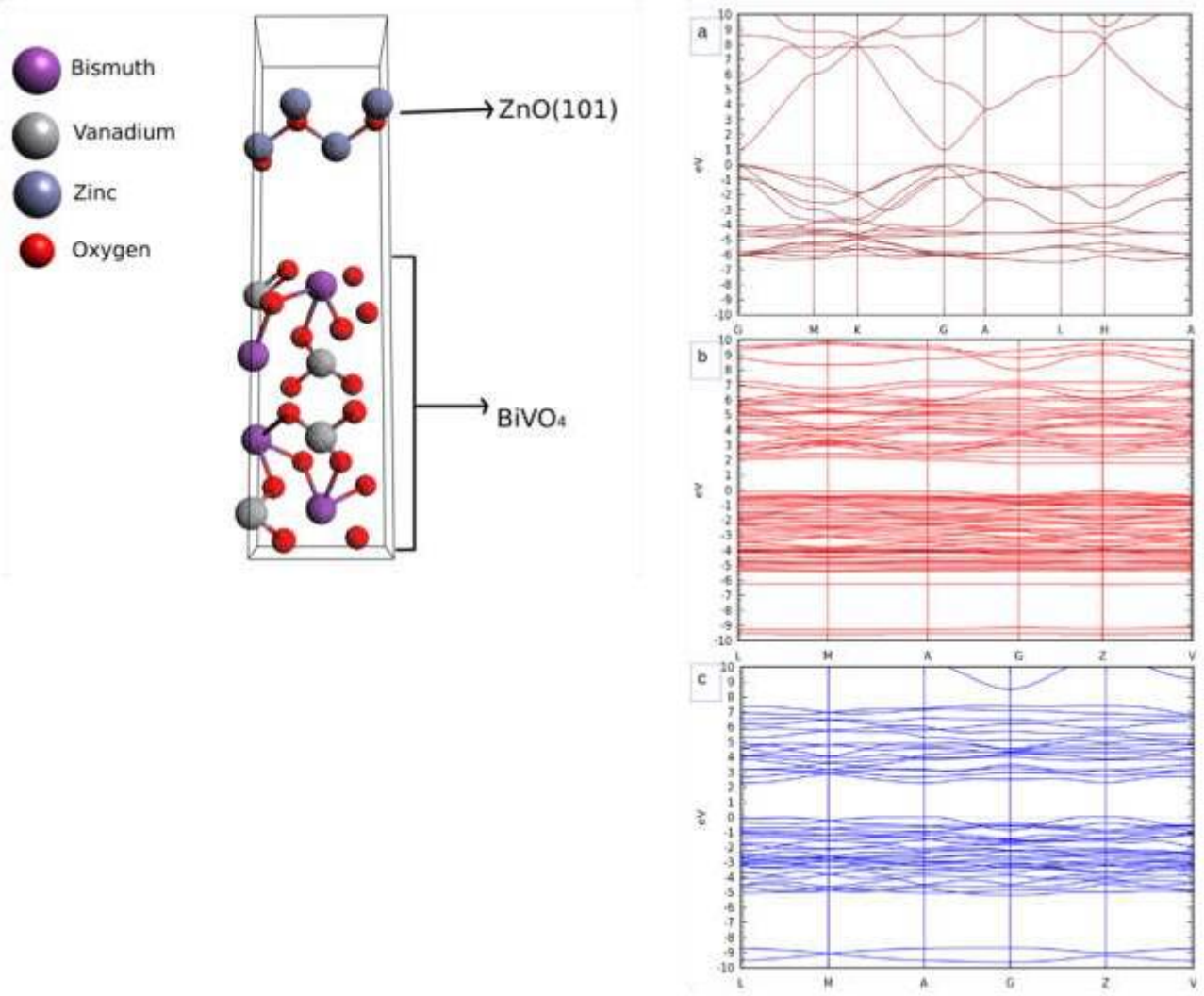

Fig 3.7. ZnO(101)-$BiVO_4$ hetrojunction optimized geometrical structure (left) & Fig 3.8. Calculated band structures of (a) Zno, (b) $BiVO_4$, and (c) ZnO-$BiVO_4$ heterojunction (right)

Further, total density of states (TDOS) and project density of states (PDOS) were calculated as shown in Fig 3.9(a), (b) and (c). Below Fermi level at 0 eV, in ZnO(101) valence band was formed by Zn s, Zn p and O p orbitals. Valence band in $BiVO_4$ mainly consisted of Bi s and O p orbital. Above the Fermi level, conduction band of ZnO(101) was formed by Zn s and in $BiVO_4$ it was mainly formed by Bi p, O p and V d orbitals. In ZnO(101)-$BiVO_4$ hetrojunction, valence band maximum was mainly occupied by Bi s orbital and conduction band minimum was occupied by Zn s orbital which indicates the maximum electron transition from $BiVO_4$ valence band to ZnO conduction band in ZnO-$BiVO_4$ composite as also confirmed by photoluminescence study.

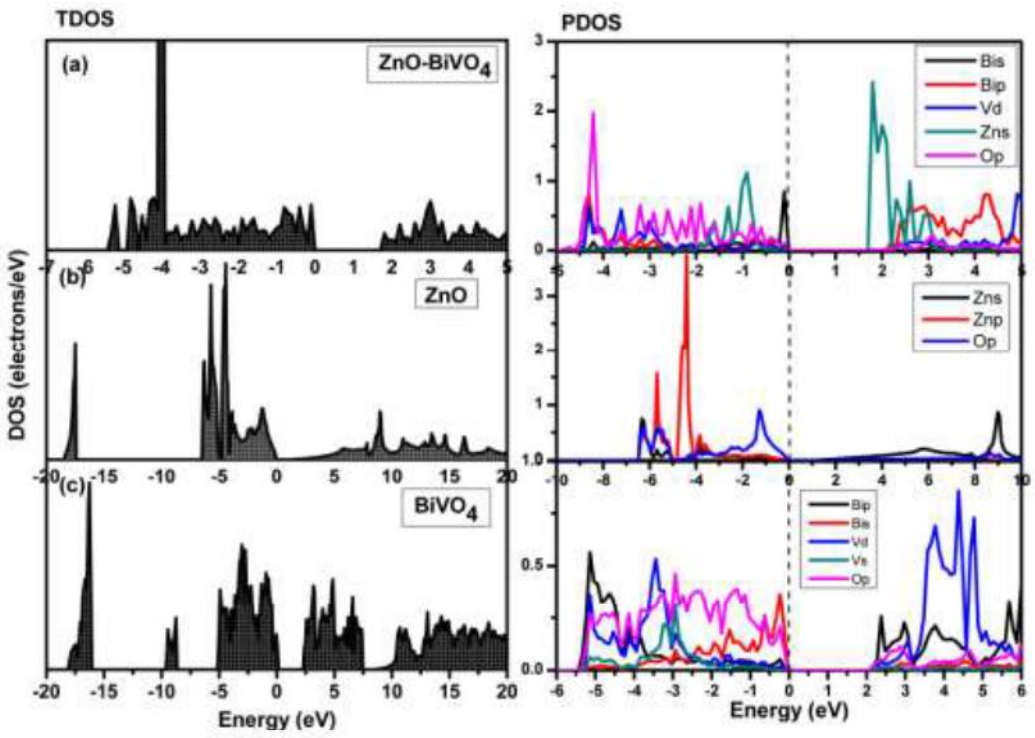

Figure 3.9 Calculated TDOS and PDOS of (a) ZnO-$BiVO_4$ heterojunction (b) ZnO (c) $BiVO_4$ heterojunction. The vertical line is Fermi level.

3.2 Photo-electrochemical Study

3.2.2 Result and discussion

Fig 3.10 shows the SEM micrographs of (a) pure ZnO (hexagonal wurtzite structure) and (b, c and d) B1, B2 and B3 ($BiVO_4$/ZnO photo anode) samples, respectively. The uneven distribution of $BiVO_4$ is attributed to poor surface wetting by ammonium vanadate leading to few $BiVO_4$ nucleation processes [10]. The $BiVO_4$ coverage on ZnO has increased with increased in $BiVO_4$ concentration from sample B1 to B3. These results are in support with the XRD studies.

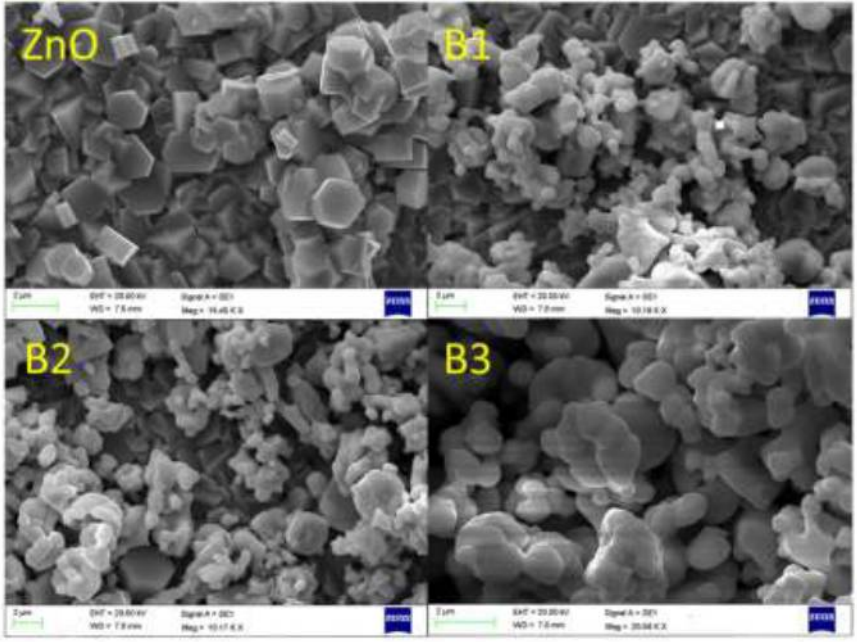

Figure 3.10 SEM micrograph of photoanode samples (a) pure ZnO (hexagonal wurtzite structure) (b) B1;$BiVO_4$ (0.035 M)/ZnO (c) B2;$BiVO_4$ (0.05 M)/ ZnO and (d) B3;$BiVO_4$ (0.1M)/ ZnO.

Figure 3.11 shows the X-ray diffractograms of pure ZnO and $BiVO_4$/ZnO (B1, B2 and B3) photoanode samples. The peaks were observed (fig. 3.11a) at 2θ (hkl): 31.76º (100), 34.42º (002), 36.25º (101), 47.53º (102), 56.60º (110), 62.86º (103), 66.37º (200), 67.96º (112) and 69.09º (201) corresponds to pure ZnO which is in good match with the JCPDS (36-1451) file number. In sample B1, B2 and B3, new set of peaks were observed at peak positions 2q(hkl): 28.87º (112), 30.53º (004), 34.51º (200), 39.87º (121), 46.01º (123), 46.77º (024), 50.18º (220), 53.32º (116), 58.39º (132), 59.69º (104), 74.64º (028), 76.04º (136); as indexed for sample B3. The observed peak positions were in good agreement with $BiVO_4$ exhibiting monoclinic phase as confirmed by JCPDS (96-901-2063) file number. Thus, the formation of monoclinic scheelite $BiVO_4$ phase is substantiated from the X-ray diffraction studies. ZnO and $BiVO_4$ peaks were differentiated using closed rhombus (◆) and open square (▯) symbols, respectively. As observed, the intensity of $BiVO_4$ peaks increases from sample B1 to B3, which is in match with the order of $BiVO_4$ concentration present in sample B1, B2 and B3.

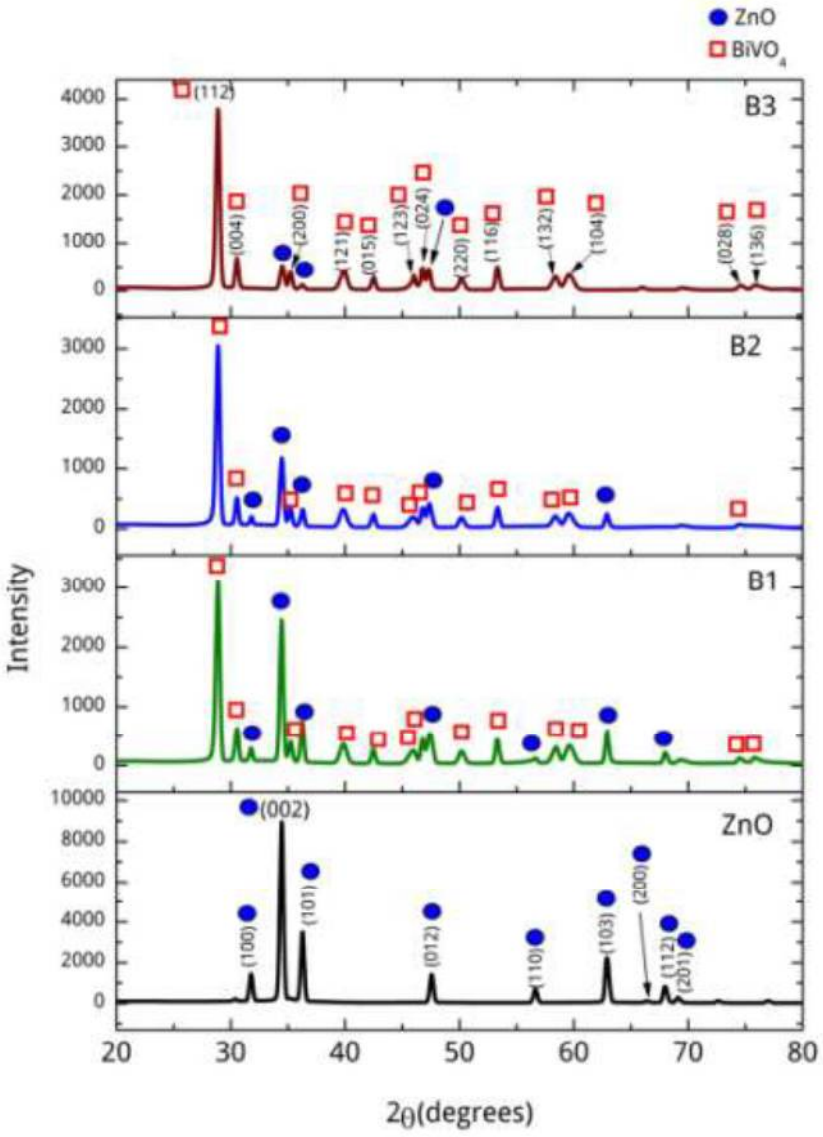

Figure 3.11: X-ray diffractogramof photoanode samples (a) pure ZnO (hexagonal wurtzite structure) (b) B1; $BiVO_4$ (0.035 M)/ZnO (c) B2; $BiVO_4$ (0.05 M)/ ZnO and (d) B3; $BiVO_4$ (0.1M)/ ZnO. ZnO and $BiVO_4$ peaks were differentiated differentiated using closed rhombus (◆) and open square (□) symbols, respectively.

The diffuse reflectance of the samples is shown in the figure 3.12. The absorption maxima for pure ZnO sample were observed to be at 373 nm, which is in good agreement with the earlier studies. In all $BiVO_4$/ZnO photoanode samples (B1, B2 and B3), strong absorption peak in the visible range of 500-800 nm was observed. As evident, absorption threshold is red-shifted in samples B1, B2 and B3 as compared to pure ZnO.

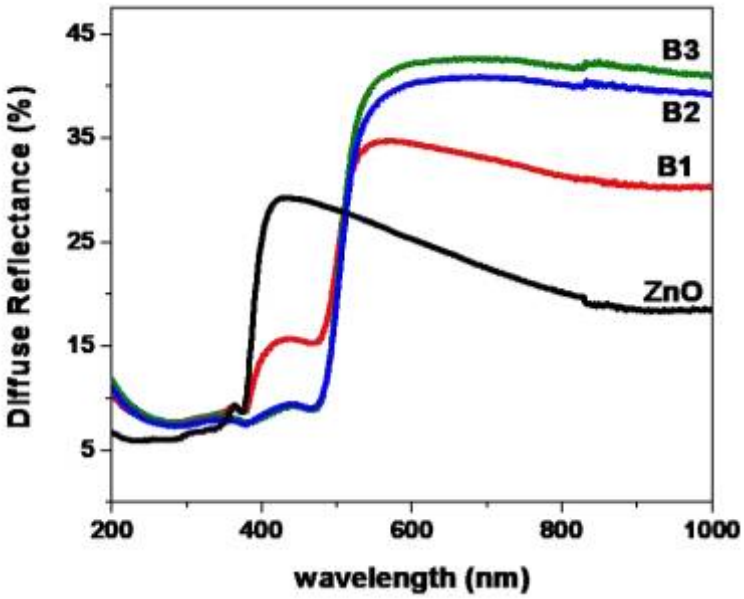

Figure 3.12. (A) Diffused reflectance spectra of photoanode samples (a) pure ZnO (b) B1;$BiVO_4$ (0.035 M)/ZnO (c) B2;$BiVO_4$ (0.05 M)/ ZnO and (d) B3;$BiVO_4$ (0.1M)/ ZnO.

4.2.3 Calculations

3.2.3.1 Estimation of Energy Band Gaps

Optical band gap was measured through Kubelka-Munk function which was calculated from diffuse reflectance spectra (DRS). Formula used for Kubelka-Munk function is as follows:

$$F(R_\infty) = \frac{(1-R)^2}{2R} = \frac{k}{s}$$

where, R is the reflectance of the material.

Graph was plotted between $[h\upsilon F(R_\infty)]^2$ against $h\upsilon$. A tangent intersecting horizontal X-axis is drawn to the plot. The point at which tangent intersects on the horizontal axis gives optical band gap (E_g) of the material. ZnO was found to exhibit band gap of 3.15 eV and for samples B1, B2 and B3

is same, ca. 2.42eV. The observed band gap values of $BiVO_4$/ZnO photo anode samples are in good agreement with the optical band gap value of $BiVO_4$ with monoclinic phase i.e 2.4 eV. In sample B1, two inflections are observed. An extra inflection at around 3.0 eV is ascribed to ZnO. Thus, synthesized $BiVO_4$/ZnO dual layered photo anode samples can effectively show visible-light driven photo catalytic activity.

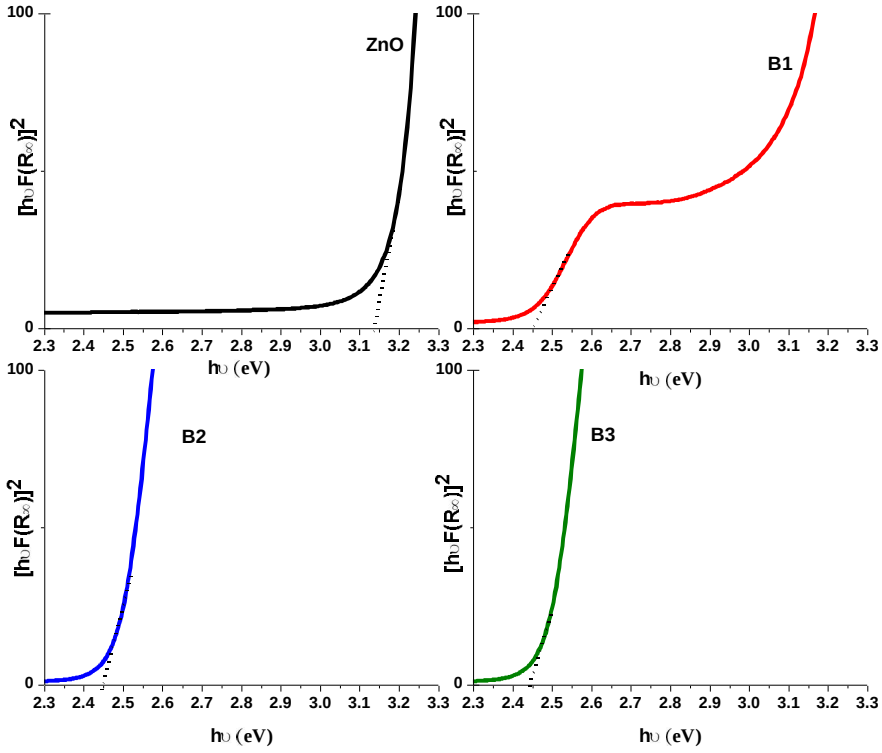

Figure 3.13 .K-M plots of photoanode samples (a) pure ZnO (b) B1;$BiVO_4$ (0.035 M)/ZnO (c) B2;$BiVO_4$ (0.05 M)/ ZnO and (d) B3;$BiVO_4$ (0.1M)/ ZnO.